Quantifying the Effect of Ankle Posture on the Positions of Bones of the Foot/Ankle Complex

Chris Smolen[1], Cheryl E. Quenneville[1,2]
[1]Department of Mechanical Engineering, McMaster University, Hamilton, ON
[2]School of Biomedical Engineering McMaster University, Hamilton, ON

ABSTRACT

The foot/ankle complex (particularly the hindfoot) is frequently injured in a wide array of debilitating events, such as car crashes. Numerical models and experimental tests have been used to assess injury risk, but most do not account for the variations in ankle posture that frequently occur during these events. In this study, the positions of the bones of the foot/ankle complex (particularly the hindfoot) were quantified over a range of postures. Computed Tomography (CT) scans were taken of a male cadaveric leg under axial loading with the ankle in five postures for which fractures are commonly reported. The difference in the location of the talus and calcaneus between the neutral and each repositioned posture was quantified, and substantial displacements and rotations were observed for all postures tested (talus range: 5-25˚, 2-12 mm; calcaneus range: 8-25˚, 1-24 mm). Strains were also recorded at seven locations on bones of the ankle during testing, and found to be highest in the calcaneus during inversion, and highest in the talus during eversion. These postural changes likely affect the load pathway of the foot/ankle complex, potentially reducing the fracture threshold from that of the neutral case, and changing the location of fracture. This highlights the need for injury predicting studies to account for these positional changes, and develop injury criteria under the most vulnerable conditions.

INTRODUCTION

The ankle is the most common site of injury for occupants during frontal vehicular collisions (Morris et al., 1997b). Furthermore, in combat zones such as Iraq and Afghanistan, improvised explosive devices (IEDs) are one of the greatest dangers to soldiers, and detonations from under body blasts can lead to serious damage to the ankles and lower limbs of an occupant (Ramasamy et al., 2011). Impacts with the ground after falling from a height are another common cause of ankle injury. As individual protective measures and medical care have improved over time, the number of fatalities due to such injuries have decreased (Ramasamy et al., 2011). However, the ankle contains a relatively low number of blood vessels, which means healing in this area can be poor (Haddock et al., 2013). As a result, these injuries can still be debilitating, especially in the case of IED detonations. Such injuries can require amputation and are associated with poor clinical results (Ramasamy et al., 2013). The health care costs associated with ankle damage are very high, especially if amputation and a prosthetic limb replacement are required (MacKenzie et al., 2007). This also says nothing of the impact on the quality of life of such victims. Along with loss of mobility, lower limb trauma can lead to chronic pain, which may interfere with everyday activities and the ability to remain a productive member of society (Castillo et al., 2006).

These injuries are also associated with a high incidence of emotional distress (McCarthy et al., 2003).

By understanding the factors that cause ankle injury, suitable protective systems can be designed. When implemented in military and civilian vehicles, these improved safety measures will lower the risks associated with these accidents, alleviating the financial and psychological burden on society and on individuals subjected to such injuries. Injury to the ankle in different loading scenarios has previously been evaluated experimentally and numerically with the ankle in a neutral position (Funk et al., 2002a, Yoganandan et al., 1996, Bandak et al., 2001). However, the ankle can assume a wide variety of postures during these traumatic events. This variation in ankle posture may alter the load path through the hind foot, with fractures having been noted in the tibia, fibula, talus and calcaneus (McKay and Bir, 2009). For falls involving the wrist, the orientation of the scaphoid and lunate have been found to affect both the fracture location and load in the radius (Troy and Grabiner, 2007). Therefore, it is possible that a similar mechanism may operate at the ankle. The hypothesis of this work is that ankle posture will affect the positions of the bones of the foot/ankle and the strains experienced during loading, which may alter the fracture threshold and location.

METHODS

Preparation of the Specimen

One male left cadaveric lower leg, sectioned at the tibial plateau, was used for testing. Seven strain gauge rosettes (I274-UFRA-1-23-3L, Hoskin Scientific Ltd., Burlington, ON) were placed on the bones of the foot/ankle complex in the following locations: tibia (1), fibula (2), plantar calcaneus (3), medial calcaneus (4), lateral calcaneus (5), medial talar neck (6), and talar sulcus (7). The strain locations were chosen to minimize the dissection of the specimen, and in particular the removal of soft tissues such as ligaments and tendons. Where possible, the locations coincided with, or were located close to, areas of particular vulnerability, such as fracture lines (Daftary et al., 2005). Strain gauge locations are illustrated in Figures 1 to 4.

Locations were accessed by semi-circular incisions made on the lateral and medial sides of the foot, and the areas of interest were exposed using conventional surgical techniques. Accurate positioning of the gauges was ensured by using a laser line intersecting anatomic landmarks which are easily palpated or identified visually. Both incisions were sutured, and a space was left in each incision for wires to pass through. Finally, the specimen was potted at the proximal tibia. Potting of the bone was conducted using a custom-designed potting apparatus that is capable of both holding the specimen and adjusting its alignment by turning threaded rods. In the sagittal plane, the laser was lined up with the center screws of the potting fixture and the medial malleolus, and in the frontal plane, the laser was lined up with the center screws of the potting fixture and the second toe.

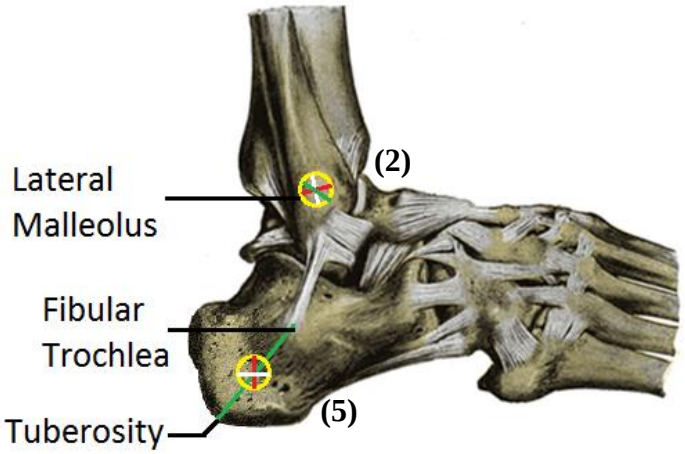

Figure 1: Strain Gauge Locations on the Lateral Side of the Foot.
A strain gauge was placed on the lateral malleolus of the fibula **(2)**, as well as the lateral calcaneal surface **(5)** midway between the tuberosity and the fibular trochlea. Rosettes are indicated in yellow, and red, white and green lines show the orientations of the gauges. Adapted from (Gray, 2009).

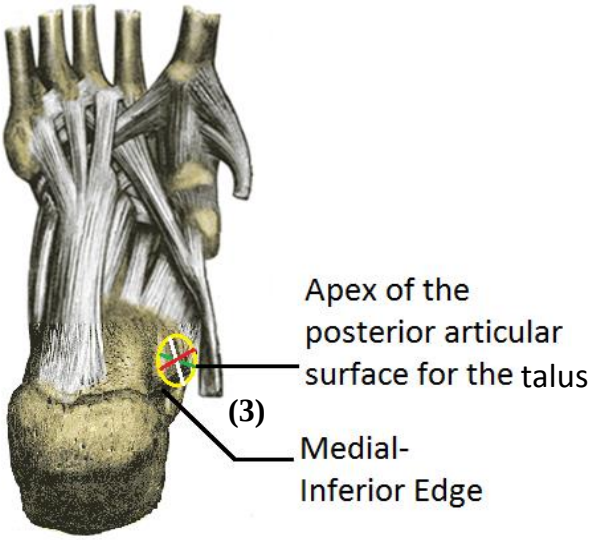

Figure 2: Strain Gauge Locations on the Plantar Surface of the Foot.
A strain gauge was placed on the plantar surface of the calcaneus **(3)** along the medial inferior edge. Rosettes are indicated in yellow, and red, white and green lines show the orientations of the gauges. Adapted from (Gray, 2009).

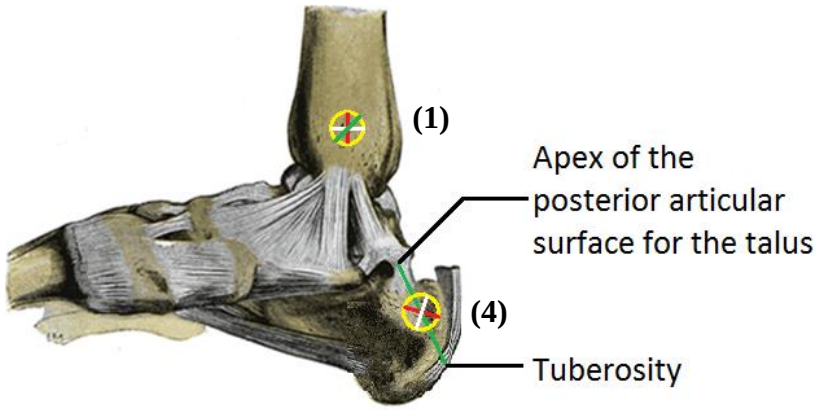

Figure 3: Strain Gauge Locations on the Medial Side of the Foot.
A strain gauge was placed on the medial malleolus of the tibia **(1)**, as well as the medial calcaneal surface **(4)** midway between the apex of the posterior articular surface for the talus and the tuberosity. Rosettes are indicated in yellow, and red, white and green lines show the orientations of the gauges. Adapted from (Gray, 2009).

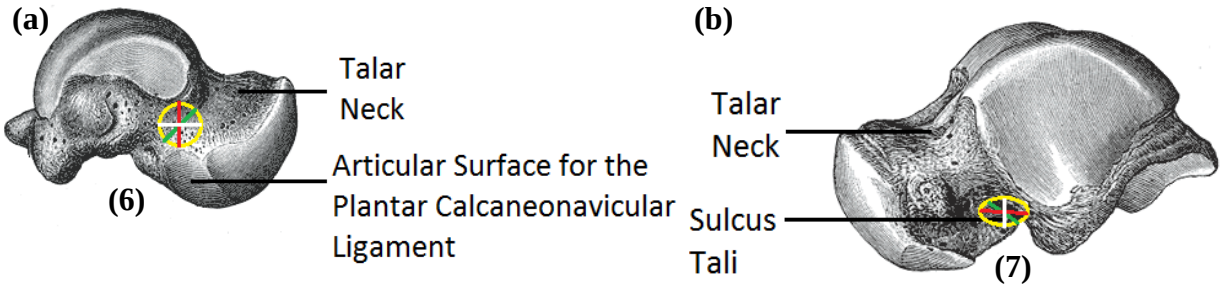

Figure 4: Talar Strain Gauge Locations
On the medial side of the talus **(a)**, a strain gauge was attached to the talar neck **(6)**. On the lateral side of the talus **(b)**, a strain gauge was attached to the talar sulcus **(7)**. Rosettes are indicated in yellow, and red, white and green lines show the orientations of the gauges. Adapted from (Gray, 2009).

Testing of the Specimen

In order to measure the precise positions of the bones of the foot, the potted leg was attached to a custom-designed CT-compatible test frame that can adjust the angles of the ankle independently in three dimensions using the ankle positioner seen in **Figure 5**. The foot rests against the foot plate of the ankle positioner and is secured via an adjustable heel brace and toe pin. Dorsiflexion and plantarflexion are controlled by rotating the footplate about the lateral-medial axis and pins are used to select the desired angle. Inversion and eversion are controlled via wedges of various inclination, which can be attached to the footplate. Internal and external rotation are controlled by the location of the toe pin, which sits between the big toe and the second toe.

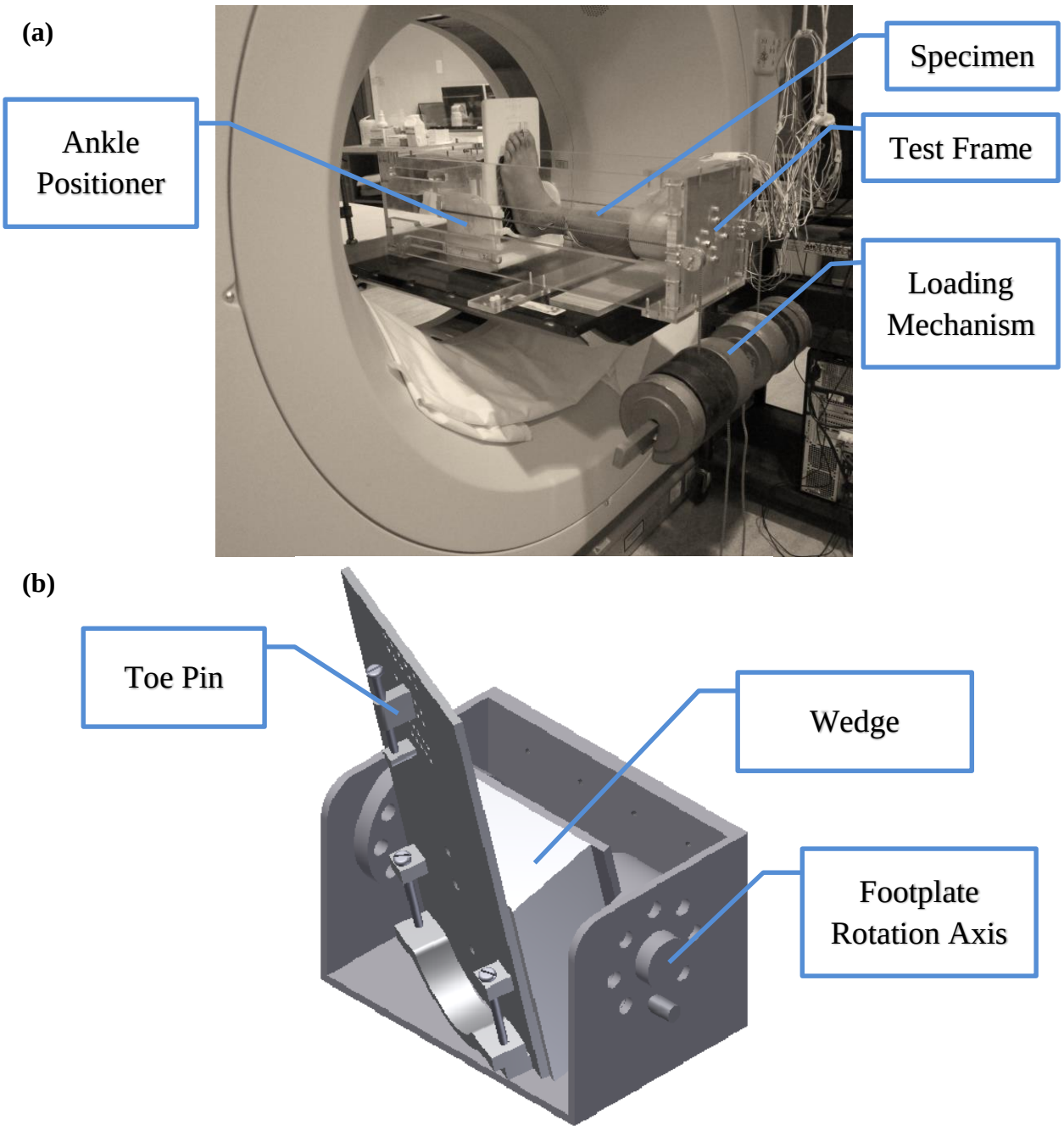

Figure 5: Experimental Setup and Test Device
The test frame **(a)** is used to adjust angle position and apply axial loading to a potted leg during CT scanning. The ankle positioner **(b)** can adjust the posture of the ankle independently in three dimensions via wedges, rotation of the footplate and toe pin position.

The test frame can apply axial loads up to 150 lbs (667 N) through the use of pulleys and hanging weights. 150 lbs was chosen as the maximum load in order to remain below failure levels

in the lower limb, but to be substantial enough to generate signals in all strain gauges (*e.g.*, (Begeman and Prasad, 1990, Funk et al., 2002a, Funk et al., 2002b)). 150 lbs is less than 20% of the failure loads reported in the aforementioned studies. As is common procedure with mechanical testing of bones (Heiner and Brown, 2001), three preconditioning cycles were applied to the specimen. In these preconditioning cycles, loads were applied from 0 to 100 lbs in 20 lb increments with the ankle in the neutral posture. Next, the leg was loaded from 0 to 150 lbs in the same increments at the neutral posture, with strain gauge readings recorded throughout the loading process. Each load was held for approximately 10 seconds in an effort to ensure loading was applied in a step-wise fashion. A CT scan (Philips Brilliance Big Bore, 120 kV, 249.48 mAs, 1 mm slick thickness) was taken approximately five minutes after the maximum load was reached.

In order to assess reproducibility of the strain measurements and ankle bone positions, the potting fixture was unscrewed and the specimen was removed from the test frame. The potting fixture was then screwed back in and the specimen reattached. The aforementioned loading protocol was repeated three more times (for a total of four tests in the neutral posture) with the potting fixture removed and reattached between each trial.

Loads were applied and CT scans were then taken for four non-neutral postures:

- 20° of inversion and 10° of external rotation
- 20° of eversion and 10° of external rotation
- 15° of dorsiflexion and 20° of inversion
- 22.5° of plantarflexion

These postures were chosen to correspond to positions that the ankle frequently assumes during injurious events, and in which fractures are commonly reported (Lauge-Hansen, 1950, Daftary et al., 2005, Sneppen et al., 1977, Morris et al., 1997a, Lestina et al., 1992). The specific dorsiflexion, inversion, eversion and external rotation angles were chosen to be on the periphery of the typical range of motion of the ankle joint (Mecagni et al., 2000, Roaas and Andersson, 1982, Nester et al., 2003). At the end of all tests, the neutral posture was retested in order to quantify any degradation of the specimen that occurred over the course of testing.

Coordinate System Development and Data Analysis

The CT scans of each posture were imported into Mimics® medical imaging software (Materialise, Leuven, Belgium) and coordinate systems were developed for the calcaneus, talus and tibiofibular complex. These coordinate systems were based on anatomic landmarks and strain gauge locations, as they show up easily on the CT scans. The coordinate systems were oriented such that the x-axis was pointed approximately in the superior direction, the y-axis in the anterior direction, and the z-axis in the lateral direction (Figure 6). The origin of the talar and calcaneal coordinate systems were chosen to be the posterior tubercle and the calcaneal notch, respectively. The origin of the tibiofibular coordinate system was selected to be a point midway between the lateral and medial malleoli.

The coordinate systems were constructed for each ankle posture and the differences between the neutral and repositioned postures were quantified based on the corresponding transformation matrices. Euler angles and the displacement of the chosen origin were calculated for each posture using an Euler Z-Y-X decomposition. Maximum principle strains were calculated for each rosette at the peak load.

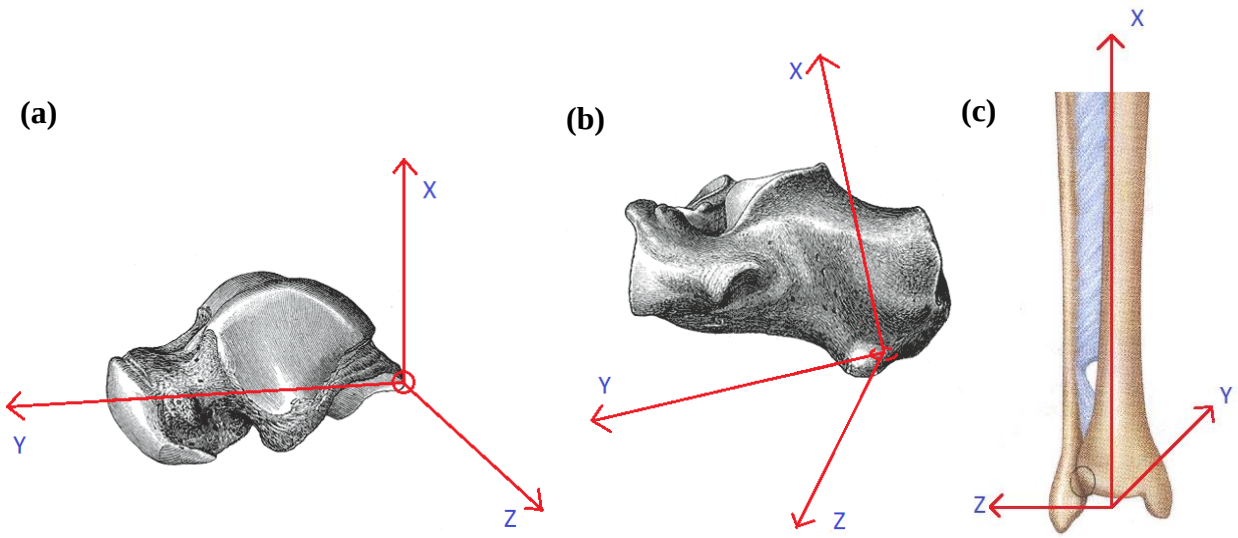

Figure 6: Bone coordinate systems.
Coordinate systems were developed for the **(a)** talus, **(b)** calcaneus and **(c)** tibiofibular complex based on strain gauge locations and anatomic landmarks that were identified on the CT scans. Adapted from (Gray, 2009) and (Maxwell, 1878).

RESULTS

The Euler angle results from the repeated neutral trials are shown in Table 1. The standard deviations of the rotations and displacements for each of the bones relative to the tibia were quite low relative to the mean. This indicates that the reproducibility of the tests was high. This table also shows the displacements and rotations for the hindfoot bones relative to the tibia for the final trial in the neutral posture (after all other tests). All values were within one standard deviation of the pre-test magnitudes, except for the z-rotation of the calcaneus, which was within two standard deviations.

Table 1: Reproducibility of the Neutral Posture and Comparison with the Final Trial
The "pre" trials are presented as the mean (standard deviation) calcaneus and talus bone rotations and displacements relative to the tibia. These trials are based on the 4 neutral trials performed at the beginning of testing. The "post" trial was performed at the end of testing in the neutral posture. Tests where the "post" trial was within one standard deviation of the "pre" trials are in black, and within two standard deviations are indicated in red.

	Calcaneus		**Talus**	
	Pre	**Post**	**Pre**	**Post**
Displacement (mm)	73.5 (0.7)	73.3	25.4 (0.5)	25.4
Z-Rotation (°)	**-7.5 (0.7)**	**-6.1**	-9.7 (1.1)	-9.2
Y-Rotation (°)	13.3 (2.3)	14.5	-8.1 (1.9)	-6.2
X-Rotation (°)	-13.6 (0.7)	-13.0	-16.7 (0.5)	-16.2

Maximum principal strains that were recorded by the strain gauges are presented in Figure 7. For the neutral posture, strains were averaged over the multiple trials and the standard deviation was calculated. These standard deviations are represented by the error bars in Figure 7. Standard deviations were less than 65 με.

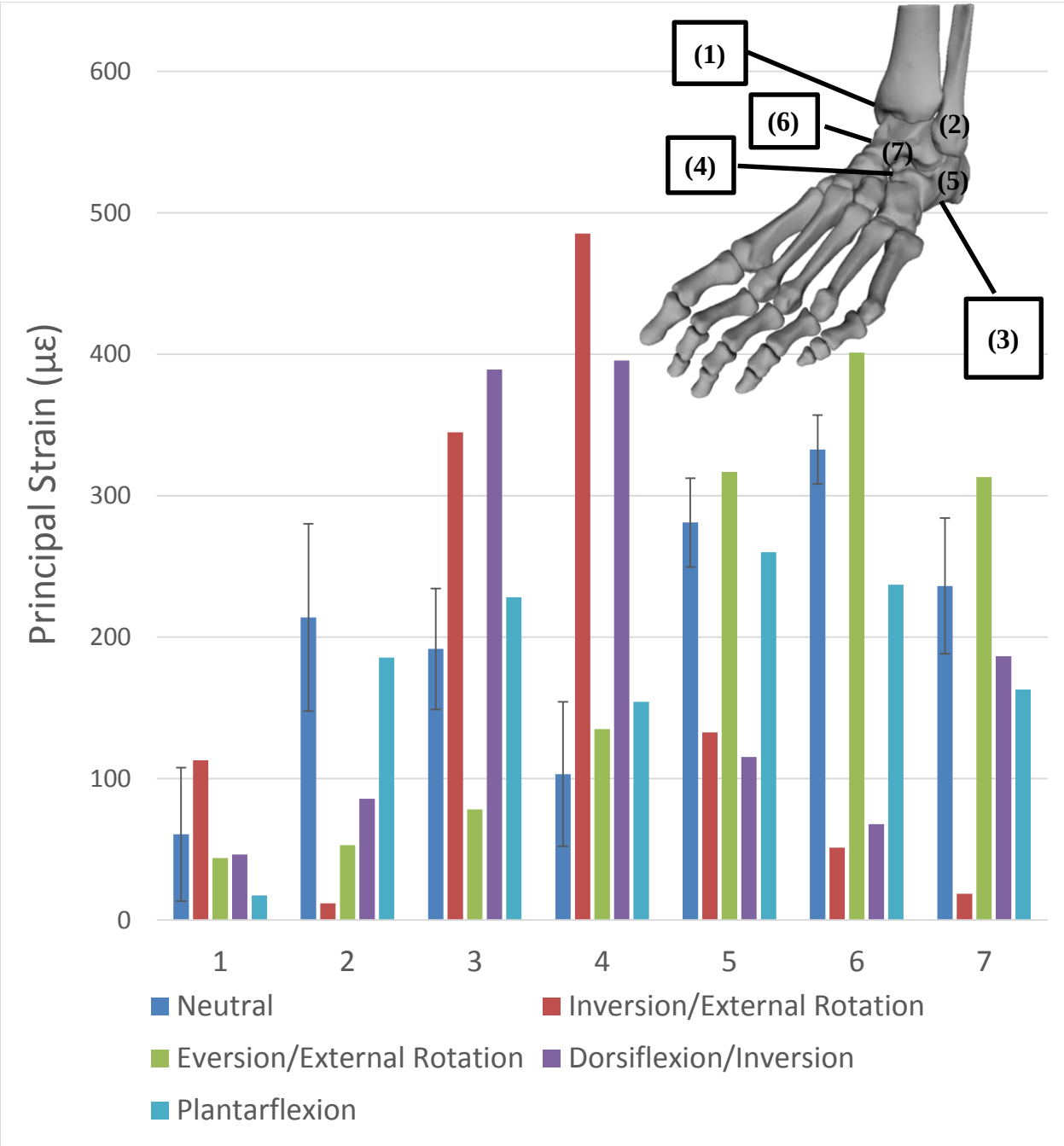

Figure 7: Strain Readings at Each Position for the Tested Postures

Peak strains at 150 lbs are presented for each of the tested postures. For the neutral posture, peak strains were averaged over the various trials and standard deviations are presented as error bars. The numbers correspond to the following strain gauge locations: tibia **(1)**, fibula **(2)**, plantar calcaneus **(3)**, medial calcaneus **(4)**, lateral calcaneus **(5)**, medial talar neck **(6)**, and talar sulcus **(7)**.

The maximum Euler angles and displacements that were observed and the corresponding ankle positions are summarized in Table 2.

Table 2: Maximum Euler Angles and Displacements of the Chosen Origin
The largest rotations and displacements for the calcaneus and talus occurred during plantarflexion and dorsiflexion, respectively.

	Calcaneus	**Talus**
Max Angle	21° in plantarflexion about Z	24° in inversion-dorsiflexion about Z
Max Displacement	24.2 mm in plantarflexion	12.0 mm in inversion-dorsiflexion

For angles of plantarflexion and dorsiflexion, the talus and calcaneus appear to rotate together for nearly the full range of motion about the z-axis (the axis that is the most closely aligned with the plantarflexion/dorsiflexion motion). For 22.5° of plantarflexion and 17.5° of dorsiflexion, the calcaneus and talus both rotated by approximately this amount about the Z-axis.

For angles of inversion and eversion, only the calcaneus rotated noticeably about the y-axis (the axis most closely aligned with the inversion/eversion motion). For 20° of inversion (coupled with 17.5° of dorsiflexion), the calcaneus only rotated about one half of this inversion value. In this case, the talus actually went through an eversion of 6°, meaning it rotated in the opposite direction to the calcaneus. For 20° of inversion (coupled with 10° of external rotation) the calcaneus only rotated about one half of this value once again. Talus rotation was negligible about the y-axis in this case. For 20° of eversion (coupled with 10° of external rotation), the calcaneus only rotated about one quarter of this eversion value, with talus rotation being negligible once again.

10° of external rotation of the ankle, when coupled with 20° of inversion, caused the calcaneus and talus to rotate by 2.5° and 7.5° respectively about the x-axis (the axis that is the most closely aligned with external/internal rotation). However, for 10° of external rotation coupled with 20° of eversion, the calcaneus rotated this full amount about the x-axis but the talus only rotated by 4°.

Across all postures, the fibula, and especially the tibia, seemed to exhibit the consistently lowest recorded strain values. The calcaneus and talus bones both exhibited relatively high strains depending on the posture being tested. In the neutral posture, the strains recorded on all bones except for the tibia were moderate compared with the other postures, but relatively comparable. The strains at the fibula, plantar calcaneus, medial talar neck and talar sulcus were especially similar.

In the inversion and external rotation posture, the medial and plantar calcaneal gauges exhibited the highest strain values. In fact, the highest strain value observed during this entire

study was recorded by the medial calcaneal gauge in this posture. While still relatively low, the tibia exhibited its highest recorded strain value in this posture. Loads on the talar neck and fibula were the lowest in this posture compared with the four other postures. In the eversion and external rotation posture, the lateral calcaneus, medial talar neck and talar sulcus all exhibited relatively high principal strains. Low strains were observed on the plantar and medial surfaces of the calcaneus, as well as the tibia. In the dorsiflexion and inversion posture, relatively high strains were observed on the plantar and medial calcaneal surfaces, as well as moderate strains on the talar sulcus. Strains on the tibia, fibula and medial talar neck were low. In the plantarflexion posture, the strain distribution was similar to that of the neutral posture. The strains recorded on the tibia, fibula and calcaneus were all within the mean ± standard deviation range of the strains observed in the neutral posture. The one difference was that strains on the talar neck were lower than those observed in the neutral posture.

DISCUSSION

To our knowledge, this study presents the most extensive analysis of how the positions of the bones of the ankle vary with posture. Furthermore, strain gauges attached to the bones of the hindfoot allowed for the observation of how the load path is altered through the ankle as posture is adjusted.

The neutral posture demonstrated good reproduciblity as the standard deviations for the positions of the talus and calcaneus were small relative to their means for the four neutral trials. Most values for the final neutral trial were within one standard deviation of the four neutral trials, indicating that no substantial damage occurred throughout the course of testing. The positional standard deviations were so small that the one value that was outside the standard deviation differed from the mean by only 1.4°, and may be more the result of landmark identification errors than damage accumulation.

For the strains recorded over the four neutral trials, the standard deviations were relatively small; however, for locations with small means the standard deviations represented large percentage variations. This is likely due to the fact that in order to conform to the irregular geometry of the ankle bones, gauges of very small gauge length (1 mm) had to be used. Strain gauges of gauge length less than 3 mm have been known to exhibit less stable behavior (Intertechnology, 2013). Overall, for the two primary bones of interest in this study though (the talus and calcaneus) the strain variation was considered to be acceptable.

The talocrural joint's main purpose seems to be to accomplish dorsiflexion and plantarflexion of the ankle. As a result, the calcaneus and talus both moved relatively freely for these types of rotations. However, for inversion and eversion, only the calcaneus contributed to the motion, indicating that the talo-calcaneal joint at least partly controls inversion and eversion of the ankle. By inspection of the CT scans, the rest of the movement seems to be accomplished mostly by the forefoot. The lower range of motion in the eversion/inversion directions suggests that the injury risk may be heightened in this posture. Figure 8 shows CT images comparing the talocalcaneal joint in the neutral and eversion-external rotation positions.

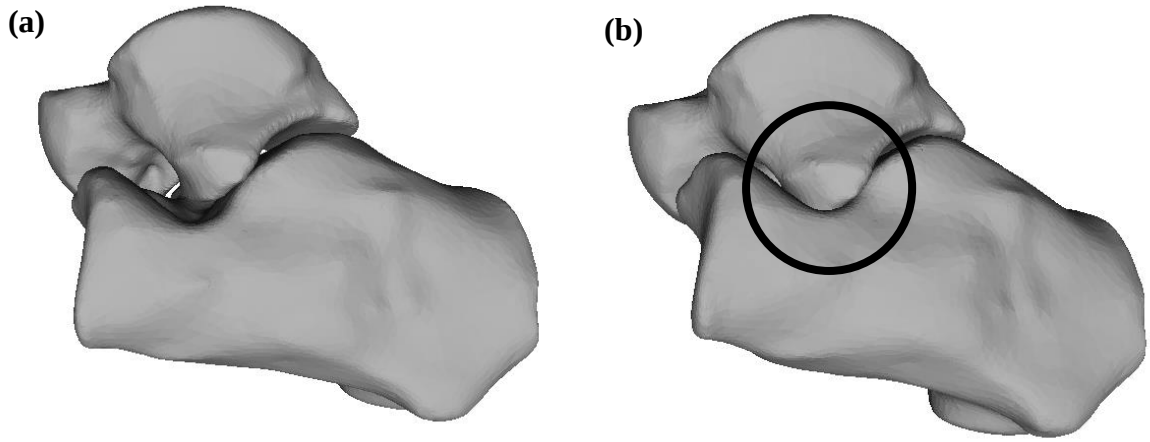

Figure 8: The Lateral Aspect of the Talo-Calcaneal Joint
Comparison of the talo-calcaneal joint for the **(a)** neutral and **(b)** inversion/external rotation postures show that the anterolateral process of the talus is being wedged into the angle of Gissane of the calcaneus. This area is circled in black.

This image shows that the talo-calcaneal joint has been completely compressed and cannot move any further. The joint is now rigid and this rigidity may contribute to a possible higher risk of injury elsewhere in the ankle, such as the lower tibia or fibula. Such behaviour has been observed previously in the Lauge-Hansen classification of ankle fracture, which is used in clinical practice to categorize ankle fractures based on the foot position and the force applied. Furthermore, 75% of calcaneal fractures can be attributed to axial loading when the anterolateral process of the talus is wedged into the angle of Gissane of the calcaneus (Carr et al., 1989), which is what is illustrated here. Similarly, axial loading and inversion have been implicated in causing fractures of the sustentaculum, located on the opposite side of the calcaneus to the angle of Gissane (Essex-Lopresti, 1952). While no strain gauge was specifically placed on the sustentaculum, the medial calcaneal gauge recorded some of the highest strains observed in this study in the two postures that involved inversion.

External and internal rotations of the ankle are the least investigated and most poorly understood ankle rotations in the literature, and several other joints of the foot and ankle have also been implicated in contributing to this motion (Lundberg, 1989). The results of this study showed that the calcaneus and talus both contribute, but the relative level of involvement of each bone changes depending on what other movements are involved.

The lowest strain values were consistently observed in the tibia and fibula. This may indicate that studies that have looked at the fracture tolerance of the tibia alone may be underestimating the absolute fracture threshold of the entire lower limb (*e.g.* (Mo et al., 2012)).

In the neutral posture, strains recorded at the fibula, plantar calcaneus, medial talar neck and talar sulcus were all very similar. Previous studies attempting to discern the mechanisms of fracture of the different bones of the ankle found that the same loading conditions often produce a

wide variety of fractures throughout this region (e.g. (McKay and Bir, 2009)). This uniformity of strains may be a contributing factor to these findings.

Inversion and external rotation generated the highest tibial strains, as well as high strains at the plantar calcaneal gauge (located medially) and medial calcaneal gauge. This seems to indicate that the principal loading is through the medial compartment of the foot and ankle in this case. Talar neck strains were low. However, inspection of the CT scans shows that the talus naturally points approximately midway between the lateral and anterior anatomical directions. As a result, the neck is oriented away from the load path, and it is possible that the body of the talus takes the majority of loading in this case.

Eversion and external rotation generated high strains in the lateral calcaneal gauge, as well the two gauges on the talar neck. This seems to indicate that the principal loading is through the lateral compartment of the foot and ankle in this case. While historically talar neck fractures were thought to be caused by combined axial compression and dorsiflexion, this has been disputed in recent years (Smith and Ziran, 1999). The results from the present study indicate that eversion causes the greatest strain on the talar neck.

Dorsiflexion and inversion generated a similar strain pattern to inversion and external rotation, suggesting that the primary load path is through the medial compartment of the leg once again. The one difference is that higher strains were observed in this posture at the talar sulcus. This may be a result of the dorsiflexion, which has been implicated in causing talar neck fractures (Daniels and Smith, 1993). However, these strains are still much lower than those observed at the talar neck during eversion and external rotation.

The strains during plantarflexion were less than or equal to those at the neutral posture for all strain gauge positions. This is consistent with previous research that has indicated that plantarflexion is not often implicated in causing ankle fractures (Smith and Ziran, 1999, Daftary et al., 2005, Lauge-Hansen, 1950).

The main limitation with this study is that only one specimen was used. Due to biological variability among people, the positional data acquired may not be applicable to the population at large. The interosseous ligament had to be sacrificed during the dissection process. There may have been some measurement error in the reading of the strain gauge and anatomic landmark locations from the CT scans during the construction of the coordinate systems in each posture. Steps were taken to minimize these errors, including having one author conduct all identifications in a single sitting. Some error may have been introduced into strain readings since very small gauges had to be used, which are known to exhibit unstable behaviour (Intertechnology, 2013). Strain gauges were also not necessarily located at locations of maximum strain, but their locations were selected to be close to known fracture sites. Finally, there are countless combinations of ankle positions and rotation angles that are possible, but this study only focused on four. The chosen postures were selected due to their prevalence in injurious events and because, in most cases, they represented the ends of the range of motion of the ankle. As a result, the effects of altering ankle posture would be more easily observed in these positions. Furthermore, the number of postures tested had to be limited due to time constraints for the CT scans and the critical thaw

time of the cadaveric leg. Reproducibility of the non-neutral postures could also not be assessed due to these time constraints.

The large rotations, displacements and strain variations for the ankle bones in the postures that were tested emphasize the need for the construction of a FE model of the ankle that accounts for this variation in posture, as well as for experimentally-determined injury criteria to test these vulnerable postures. The displacements and rotations of the bones of the hind foot appear to affect the load pathway of the foot/ankle complex under axial loading, potentially reducing the fracture threshold and changing the location of fracture. This effect does not appear to have been previously investigated in the literature, and the results from this study will be useful in determining injury limits of the ankle and for developing postural guidelines to minimize injury.

ACKNOWLEDGEMENTS

This research is funded by the National Sciences and Engineering Research Council of Canada, the Canada Founding for Innovation, the Ontario Research Fund, the Ontario Graduate Scholarship Program and McMaster University. We would also like to thank Dr. Harjeet Gandhi for his assistance during the dissection of the specimen and Dr. Tom Chow for his help in performing the CT scans and setting up the test frame in the CT scanner.

REFERENCES

BANDAK, F., TANNOUS, R. & TORIDIS, T. 2001. On the development of an osseo-ligamentous finite element model of the human ankle joint. *International journal of solids and structures,* 38**,** 1681-1697.

BEGEMAN, P. C. & PRASAD, P. 1990. Human ankle impact response in dorsiflexion. SAE Technical Paper.

CARR, J. B., HAMILTON, J. J. & BEAR, L. S. 1989. Experimental intra-articular calcaneal fractures: anatomic basis for a new classification. *Foot & Ankle International,* 10**,** 81-87.

CASTILLO, R. C., MACKENZIE, E. J., WEGENER, S. T. & BOSSE, M. J. 2006. Prevalence of chronic pain seven years following limb threatening lower extremity trauma. *Pain,* 124**,** 321-329.

DAFTARY, A., HAIMS, A. H. & BAUMGAERTNER, M. R. 2005. Fractures of the Calcaneus: A Review with Emphasis on CT 1. *Radiographics,* 25**,** 1215-1226.

DANIELS, T. R. & SMITH, J. W. 1993. Talar neck fractures. *Foot & Ankle International,* 14**,** 225-234.

ESSEX-LOPRESTI, P. 1952. The mechanism, reduction technique, and results in fractures of the os calcis. *British Journal of Surgery,* 39**,** 395-419.

FUNK, J. R., CRANDALL, J. R., TOURRET, L. J., MACMAHON, C. B., BASS, C. R., PATRIE, J. T., KHAEWPONG, N. & EPPINGER, R. H. 2002a. The axial injury tolerance of the human foot/ankle complex and the effect of Achilles tension. *Journal of biomechanical engineering,* 124**,** 750-757.

FUNK, J. R., SRINIVASAN, S. C., CRANDALL, J. R., KHAEWPONG, N., EPPINGER, R. H., JAFFREDO, A. S., POTIER, P. & PETIT, P. Y. 2002b. The effects of axial preload and dorsiflexion on the tolerance of the ankle/subtalar joint to dynamic inversion and eversion. SAE Technical Paper.

GRAY, H. 2009. *Gray's Anatomy: With original illustrations by Henry Carter*, Arcturus Publishing.

HADDOCK, N. T., WAPNER, K. & LEVIN, L. S. 2013. Vascular bone transfer options in the foot and ankle: a retrospective review and update on strategies. *Plastic and reconstructive surgery,* 132**,** 685-693.

HEINER, A. D. & BROWN, T. D. 2001. Structural properties of a new design of composite replicate femurs and tibias. *Journal of Biomechanics,* 34**,** 773-781.

INTERTECHNOLOGY 2013. Strain Gage Selection: Criteria, Procedures, Recommendations.

LAUGE-HANSEN, N. 1950. Fractures of the ankle: II. Combined experimental-surgical and experimental-roentgenologic investigations. *Archives of Surgery,* 60**,** 957-985.

LESTINA, D. C., KUHLMANN, T. P., KEATS, T. E. & ALLEY, R. M. 1992. Mechanisms of fracture in ankle and foot injuries to drivers in motor vehicle crashes. SAE Technical Paper.

LUNDBERG, A. 1989. Kinematics of the ankle and foot: in vivo roentgen stereophotogrammetry. *Acta Orthopaedica,* 60**,** 1-26.

MACKENZIE, E. J., CASTILLO, R. C., JONES, A. S., BOSSE, M. J., KELLAM, J. F., POLLAK, A. N., WEBB, L. X., SWIONTKOWSKI, M. F., SMITH, D. G. & SANDERS, R. W. 2007. Health-care costs associated with amputation or reconstruction of a limb-threatening injury. *The Journal of Bone & Joint Surgery,* 89**,** 1685-1692.

MAXWELL, J. C. 1878. Encyclopedia Britannica. Samuel L. Hall, New York, NY.

MCCARTHY, M. L., MACKENZIE, E. J., EDWIN, D., BOSSE, M. J., CASTILLO, R. C., STARR, A., KELLAM, J. F., BURGESS, A. R., WEBB, L. X. & SWIONTKOWSKI, M. F. 2003. Psychological distress associated with severe lower-limb injury. *The Journal of Bone & Joint Surgery,* 85**,** 1689-1697.

MCKAY, B. J. & BIR, C. A. 2009. Lower extremity injury criteria for evaluating military vehicle occupant injury in underbelly blast events. *Stapp car crash journal,* 53**,** 229.

MECAGNI, C., SMITH, J. P., ROBERTS, K. E. & O'SULLIVAN, S. B. 2000. Balance and ankle range of motion in community-dwelling women aged 64 to 87 years: a correlational study. *Physical Therapy,* 80**,** 1004-1011.

MO, F., ARNOUX, P. J., JURE, J. J. & MASSON, C. 2012. Injury tolerance of tibia for the car–pedestrian impact. *Accident Analysis & Prevention,* 46**,** 18-25.

MORRIS, A., THOMAS, P., TAYLOR, A. M. & WALLACE, W. A. 1997a. Mechanisms of fractures in ankle and hind-foot injuries to front seat car occupants-an in-depth accident data analysis.

MORRIS, A., THOMAS, P., TAYLOR, A. M. & WALLACE, W. A. MECHANISMS OF FRACTURES IN ANKLE AND HIND-FOOT INJURIES TO FRONT SEAT CAR OCCUPANTS: AN IN-DEPTH ACCIDENT DATA ANALYSIS. PROCEEDINGS OF THE 41ST STAPP CAR CRASH CONFERENCE, NOVEMBER 13-14, 1997, ORLANDO, FLORIDA, USA (SAE TECHNICAL PAPER 973328), 1997b.

NESTER, C. J., FINDLOW, A. F., BOWKER, P. & BOWDEN, P. D. 2003. Transverse plane motion at the ankle joint. *Foot & ankle international,* 24**,** 164-168.

RAMASAMY, A., MASOUROS, S. D., NEWELL, N., HILL, A. M., PROUD, W. G., BROWN, K. A., BULL, A. M. & CLASPER, J. C. 2011. In-vehicle extremity injuries from

improvised explosive devices: current and future foci. *Philosophical Transactions of the Royal Society B: Biological Sciences,* 366**,** 160-170.
RAMASAMY, M. A., HILL, C. A. M., MASOUROS, S., GIBB, L.-C. I., PHILLIP, L.-C. R., BULL, A. M. & CLASPER, C. J. C. 2013. Outcomes of IED Foot and Ankle Blast Injuries. *The Journal of Bone & Joint Surgery,* 95**,** e25 1-7.
ROAAS, A. & ANDERSSON, G. B. 1982. Normal range of motion of the hip, knee and ankle joints in male subjects, 30-40 years of age. *Acta Orthopaedica,* 53**,** 205-208.
SMITH, P. N. & ZIRAN, B. H. 1999. Fractures of the talus. *Operative techniques in orthopaedics,* 9**,** 229-238.
SNEPPEN, O., CHRISTENSEN, S. B., KROGSØE, O. & LORENTZEN, J. 1977. Fracture of the body of the talus. *Acta Orthopaedica,* 48**,** 317-324.
TROY, K. L. & GRABINER, M. D. 2007. Off-axis loads cause failure of the distal radius at lower magnitudes than axial loads: a finite element analysis. *Journal of biomechanics,* 40**,** 1670-1675.
YOGANANDAN, N., PINTAR, F. A., BOYNTON, M., BEGEMAN, P., PRASAD, P., KUPPA, S. M., MORGAN, R. M. & EPPINGER, R. H. 1996. Dynamic axial tolerance of the human foot-ankle complex. SAE Technical Paper.